GEOLOGICAL JOURNAL
*Geol. J.* **45**: 170–185 (2010)
Published online 21 July 2009 in Wiley InterScience
(www.interscience.wiley.com) DOI: 10.1002/gj.1168

# Evidence for sea-level falls in the Permian-Triassic transition in the Ziyun area, South China

***WU YA-SHENG*, JIANG HONG-XIA and FAN JIA-SONG***

*Institute of Geology and Geophysics, Chinese Academy of Sciences, Beijing, China*

The sedimentology of three sections showing the Permian–Triassic (P–T) transition on an Upper Permian reef in Ziyun, Guizhou Province, southwest China provides evidence of sea-level fall in this area. The P–T transition in the Gendan section, which covers a reef-front sequence, contains a subaerial exposure surface and various desiccation cracks (including rolled-up chips, in-chip cracks, pyramid cracks, vertical cracks and sheet cracks), indicating sea-level falls. The P–T transition in the Shitouzhai section, which covers a reef-core sequence, contains three micritic beds with abundant pseudomorphs of tabular gypsum crystals replaced by calcite. The underlying centimetres of deposits are composed of fine-crystalline dolostone, and have a sharp contact with the underlying reef-core facies. The association of gypsum pseudomorphs and fine-crystalline dolostone suggests an origin related to a supratidal evaporative environment. The P–T transition in the Tanluzhai section, which covers a back-reef sequence, is fine-crystalline dolostone, and shows a laminated algal structure indicating tidal-flat environments. The middle part of the dolostone interval has become a collapse breccia composed of dolostone fragments and a matrix of micrites or crustose multi-generation calcite cements. The formation of the collapse breccia is interpreted to be related to the dissolution of the evaporite interbeds originally present between the thin dolostone beds. The formation of the evaporite deposits requires a supratidal condition.


*Received 4 September 2008; accepted 15 May 2009*

KEY WORDS Permian–Triassic boundary; P–T transition; subaerial exposure; sea-level fall; end-Permian; Ziyun; reef

## 1. INTRODUCTION

Many studies have been done on non-reef marine Permian–Triassic boundary (PTB) sections (Noé 1987; Yang *et al*. 1991; Wignall and Hallam, 1992, 1996; Kajiwara *et al*., 1994; Eshet *et al*. 1995; Schubert and Bottjer 1995; Jin *et al*. 1996; Lai *et al*. 1996; Twitchett *et al*. 2001, 2004; Yin *et al*. 1996; Isozaki 1997; Garzanti *et al*. 1998; Lehrmann *et al*. 1998, 2001, 2003; Shen and Jin 1999; Jin *et al*. 2000; Yin *et al*. 2001; Brookfield *et al*. 2003; Ezaki *et al*. 2003; Heydari *et al*. 2003; Krystyn *et al*. 2003; Wignall and Newton 2003; Grice *et al*. 2005; Xie *et al*. 2005), and some on non-marine sections (Retallack 1995; Retallack *et al*. 1998; Michaelsen 2002; Steiner *et al*. 2003; Benton *et al*. 2004; Peng *et al*. 2005; Ward *et al*. 2005), but few on PTB sections on reefs (Wignall and Hallam 1996; Kershaw *et al*. 1999, 2002). Reefs have higher elevation than surrounding coeval non-reef sedimentary units. Thus, sea-level changes may have more intense impact on reefs than on non-reef biota and environments.

There has been controversy about the sea-level changes (their types and scales) across the PTB. Yang *et al*. (1991) proposed that there is a regression in the latest Permian. Jin *et al*. (1994), however, proposed that a rapid transgression began in the latest Permian and was accompanied by sudden end-Changhsingian flooding. Wignall and Hallam (1992, 1996) proposed that the end-Permian mass extinction was caused by oceanic anoxia related to a sea-level rise across the PTB. This viewpoint has been followed by many researchers (Kershaw *et al*. 1999, 2002). Tong *et al*. (1999), however, identified a slight regression in the latest Changhsingian. Erwin *et al*. (2002) stated that a transgression began in lower to mid-Changhsingian time, and extended through the P–T boundary into the Early Triassic. Yin *et al*. (2007) proposed that a great regression happened at the P–T boundary. Up to now, no agreement has been reached about the sea-level changes during the P–T transition. The current study reveals evidence for sea-level falls in three PTB sections on an Upper Permian

* Correspondence to: W. Ya-Sheng, Institute of Geology and Geophysics, Chinese Academy of Sciences, Beijing 100029, China.
E-mail: wys@mail.igcas.ac.cn

Changhsingian reef in Ziyun, Guizhou Province, southwest China, and may be helpful to resolve this problem.

## 2. GENERAL FEATURES OF THE THREE PTB SECTIONS

A developed Upper Permian Changhsingian reef is exposed in the vicinity of Ziyun town, Guizhou Province, southwest China (Figure 1). Previous researches (Wang *et al*. 1996; Shen and Xu 2005) and our field work reveal that the reef has differentiation of back-reef, reef core and reef-front facies. Three sections across the back-reef, reef core and reef-front facies sequences respectively, the Tanluzhai, Shitouzhai and Gendan sections, have been measured (Figure 2).

The reef-core facies is well exposed in the vicinity of Qingcaichong, Daditou, Tuanshan and Tanluzhai villages, and is maximally 173.3 m thick at the Shitouzhai section (Figure 2). It is composed of framestone, bafflestone and pack-wackestone, and contains diverse reef-building calcisponges (inozoans and thalamid sponges) and sclerosponges. The micritic limestone (ML) overlying the reef-core sequence (the PTB interval defined for this section), is about 0.08 m thick, lacks any recognizable fossils or sedimentary bedding, and is covered by the alternation of thin-bedded marls and shales of the basal Feixianguan Formation. The age of the basal Feixianguan Formation is lowest Triassic age, as indicated by ammonoid fossils.


Figure 1. Location of the Upper Permian Changhsingian reef in Ziyun, Guizhou Province and southwestern China.

The reef-front facies is exposed in the vicinity of Gendan village, and has a thickness of 100.3 m at the Gendan section (Figure 2). It is mainly composed of bafflestone, framestone, pack-wackestone and grainstone, and is characterized by several beds of rudstone with abundant fragments of reef-

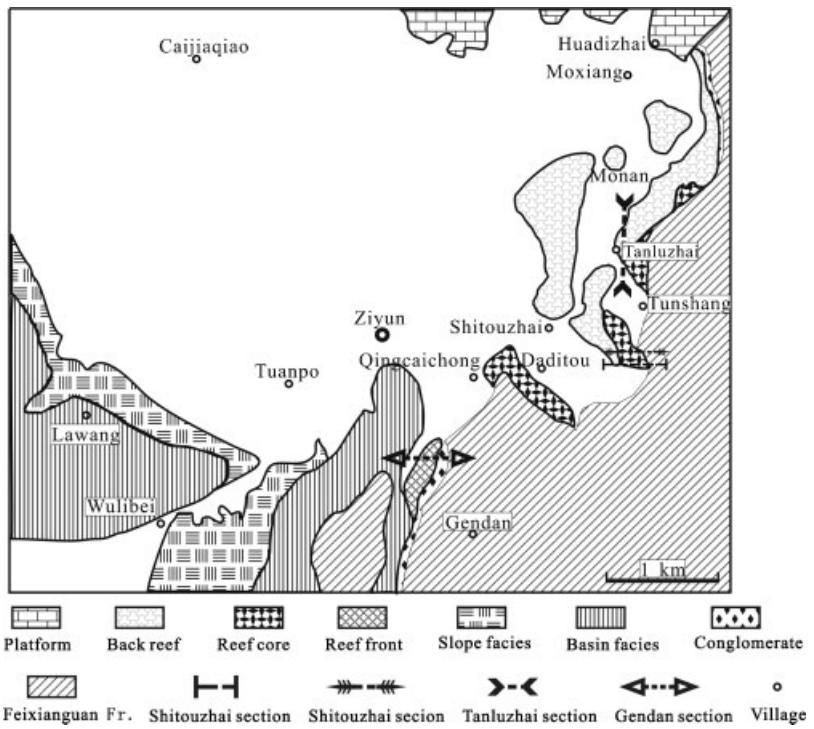


Figure 2. Outcrop distribution of different parts of the Upper Permian Changhsingian reef in Ziyun, the reef core, reef-front and back reef, and the localities of the three Permian-Triassic boundary sections studied: the Gendan, Shitouzhai and Tanluzhai sections.



DOI: 10.1002/gj

building calcisponges, the crustose alga *Archaeolithoporella* and reef rocks. The reef rock fragments may reach 15 cm in diameter, as observed on the Gendan section. The reef-front limestone was overlain by a laminated dolostone interval (the PTB interval defined for this section), which is about 3.0 m thick, and is covered by a bedded limestone containing macro-ammonoid and bivalve fossils of early Triassic age. The limestone overlying the ammonoid-bearing limestone has fine thin flat-bedding, and shows no macrofossils.

The back-reef facies is exposed in the vicinity of Monan village (Figure 2), and is 86.6 m thick at the Tanluzhai section. The lower part of the Changhsingian at the Gendan section is mainly composed of packstone and wackestone with abundant dasycladaceans and foraminifer bioclasts. Its upper part is mainly composed of framestone, with some bafflestone and rudstone containing reef-rock fragments. Since dasycladacean-foraminiferal limestone accounts for most of the thickness, the Gendan section is interpreted as back-reef facies. Dolomitic patches are present in the southern distribution of the back-reef facies, while the northern distribution has all been altered to dolostone. The back-reef facies in Tanluzhai section is overlain by a laminated dolostone interval lacking macrofossils. The thick-bedded limestone covering the laminated dolostone contains abundant macro-ammonoids of early Triassic age. Since the laminated dolostone is the interval between the Changhsingian back-reef deposits and the early Triassic ammonoid limestone, it is defined as the P–T transition of the Gendan section.

## 3. DESICCATION CRACKS IN THE PTB SECTION AT GENDAN ON A REEF-FRONT

### *3.1. Lithology*

The PTB section at Gendan is lithologically divided into 7 beds (Figure 3B). The basal Bed 1 (0.2 m) covering the reef-front sequence is a bioclastic grainstone, with fibrous calcite cements. The bioclasts include *Tubiphytes*, algae, foraminifers, fusulinids, gastropods and some echinoderms. Locally, the lithology passes into bioclastic wackestone. The fusulinid *Palaeofusulina sinensis* and foraminifer *Colaniella* are present in this bed (Wang *et al*. 1996; Shen and Xu 2005).

Bed 2 (0.8 m) is composed of fine-crystalline dolostone with relicts of skeletal grains including fusulinids, foraminifers and gastropods of the precursor bioclastic wackestone. Its top part contains abundant remnant gastropods.

Bed 3 (0.1 m) is a fine-crystalline dolostone. Its top surface is an exposure surface (Figure 4j), and contains rolled-up chips and various cracks. Some crustose phosphorite occurs on the top of this bed, generally as curved, sheet-like debris.

Bed 4 (2.3 m) is a fine-crystalline dolostone, with a wavy laminated structure resembling that of a stromatolite, composed of dark-coloured thin wavy laminae alternating with thicker lighter-coloured laminae and interpreted to be originated from algal mats. Various cracks are present in this bed.

Bed 5 (0.2 m) is a fine-crystalline dolostone, with a laminated structure. It contains small globular microbial fossils (Wu *et al*. 2007a: Figure 4), ostracods and some larger but thin-shelled bivalves. The top of this bed contains abundant ostracods. The original lithology of this bed is lime mudstone. This bed is overlain by a 1–2 mm thick layer of pyrite. Pyrite is present in the whole bed 5, and its content decreases from the top to the bottom.

Bed 6 (0.003 m) is grainstone. The grains are microgastropods and have been cemented by sparry calcite cements.

Bed 7 (0.4 m) is composed of grainstone. The grains are ammonoid and bivalve shells. Septa in ammonoid shells are generally damaged and the bivalve shells are generally disarticulated.

Bed 8 is composed of nonfossiliferous micritic mudstone, with flat beddings.

### *3.2. Biostratigraphy*

The conodont *Clarkina parasubcarinata* (Figure 4a) (Mei *et al*. 1998) has been found from Bed 1. In the PTB section of Meishan, the Global Stratotype Section and Point (GSSP) of the PTB, this conodont occurs in Bed 24e (Wu 2005), and is regarded as a key component of the *Clarkina yini* (= '*C. changxingensis yini*') (Yin *et al*. 2001; Wu 2005) conodont zone. So, our Bed 1 is correlated to the *C. yini* Zone of Meishan.

The conodont *Hindeodus parvus* (Figure 4c) has been found from Bed 5. This is a conodont that has been defined as the marker of the beginning of the Early Triassic (Yin *et al*. 2001). Thus, Bed 5 is correlative to beds 27c to 27d of Meishan, the lowermost conodont zone of the Lower Triassic. Up to now, no conodonts have been found from beds 3 and 4, and this interval is correlated to beds 26–27b of Meishan.

Bed 7 contains the bivalves *Claraia* cf. *griesbachi* (Figure 4d) and *C. griesbachi* (Figure 4e), and the ammonoid *Prionolobus impressus* (Figure 4f and g). In the Meishan section, and two previous candidates for the GSSP of PTB, the Shangsi section in Guangyuan, Sichuan Province and Guryul Ravine section in Kashmir, India, *Claraia griesbachi* is accompanied by the conodont '*Isarcicella isarcica*' (actually it is *I. staeschei*) (Yin *et al*. 1996, 2001), the index fossil of the *I. staeschei* Zone in Meishan (Wu 2005). Thus, Bed 7 of Gendan is correlative



DOI: 10.1002/gj

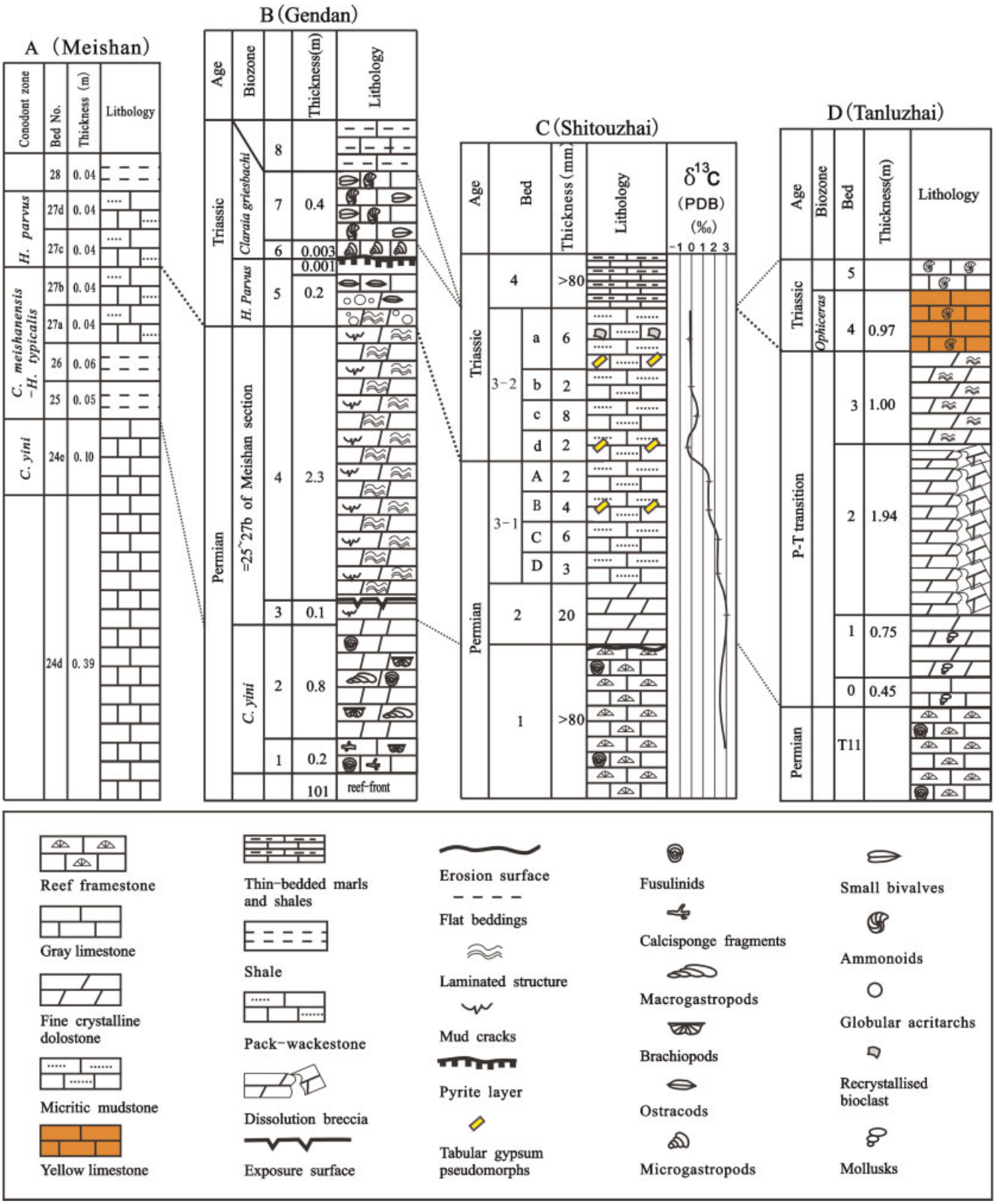


Figure 3. Stratigraphic columns of the Gendan, Shitouzhai and Tanluzhai sections and their correlation to the Meishan section. This figure is available in colour online at www.interscience.wiley.com/journal/gj



DOI: 10.1002/gj

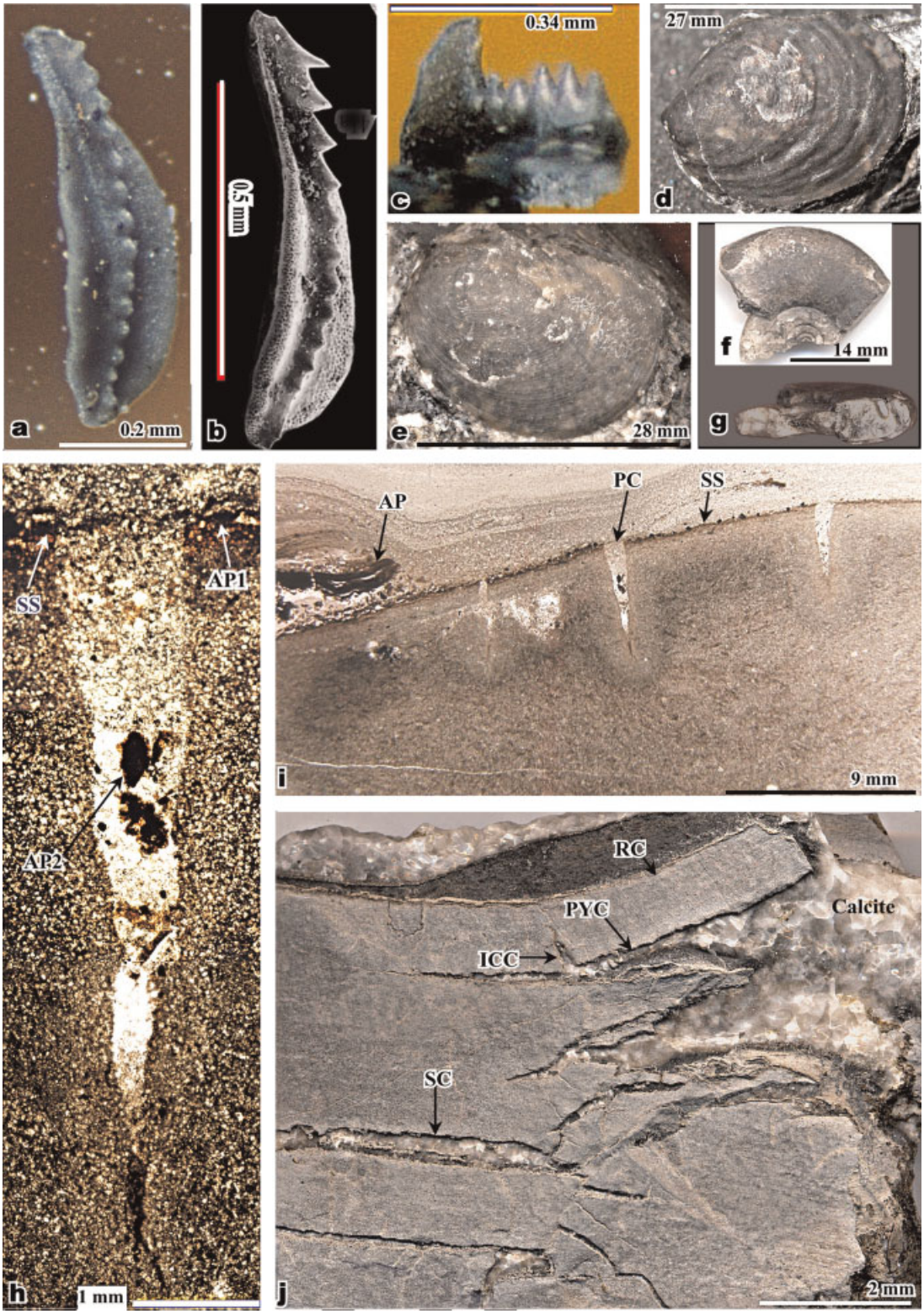


Figure 4. Fossils and sedimentological evidence for a sea-level fall in the Gendan section. (a) *Clarkina parasubcarinata*, from Bed 1. (b) Holotype of *Clarkina parasubcarinata*. (c) *Hindeodus parvus*, from Bed 5. (d) *Claraia* cf. *griesbachi*, from Bed 7. (e) *Claraia griesbachi*, from Bed 7. (f) side view and (g) cross view of *Prionolobus impressus* (Waagen), from Bed 7. (h) Enlargement of a vertical crack (PC of Figure 4i), showing its wedge-like shape and filling deposit the same as the overlying bed. The phosphorite debris (AP2) in the crack is the same as those on the exposure surface (AP1). An exposure surface (SS) is shown. (i) Vertical thin section showing exposure surface (SS), vertical cracks (PC) and debris of laminated phosphorite (AP). Deposits in cracks are the same as those on the exposure surface. (j) Outcrop showing rolled-up chip (RC), in-chip cracks (ICC), pyramid cracks (PYC) and sheet cracks (SC). The PYC looks like stacked pyramids filled with granular calcites. Parts (h)–(j) from Bed 3. This figure is available in colour online at www.interscience.wiley.com/journal/gj



DOI: 10.1002/gj

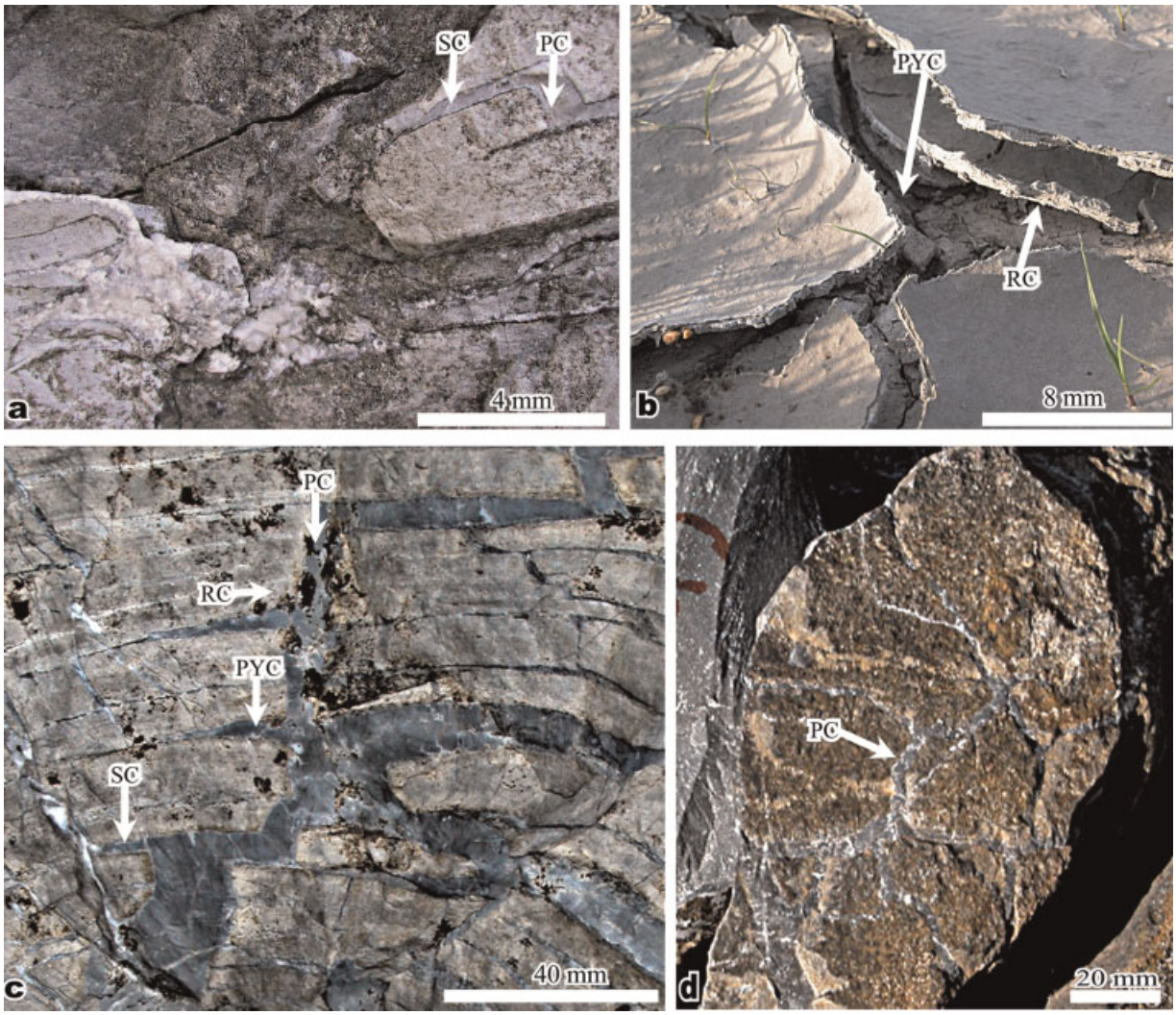


Figure 5. Sedimentological evidence for a sea-level fall in Beds 3 and 4 of the Gendan section. (a) An outcrop of Bed 3 showing sheet cracks (SC), vertical cracks (PC) and the position of the sample of Figure 4j. (b) Rolled-up chips (RC) and pyramid cracks (PYC) in a modern dried-up pond in Texas. (c) An outcrop of Bed 4 showing rolled-up chips (RC), pyramid cracks (PYC), vertical/prism cracks (PC) and sheet cracks (SC), all filled by micritic limestone. (d) A sample of Bed 4 showing polygonal cross sections of prism crack (PC). This figure is available in colour online at www.interscience.wiley.com/journal/gj

to Bed 28 of Meishan. Bed 8 contains no fossils, and its age is unknown.

### *3.3. Sedimentology and evidence for subaerial exposure*

Beds 1 and 2 contain a platform biota including fusulinids, echinoderms, and *Tubiphytes*. Beds 3 and 4 have a wavy laminated structure, probably originated from an algal mat representing a tidal flat environment.

Bed 3 has various desiccation cracks (Figures 4h, i, j and 5c) and a subaerial exposure surface (Figure 4i). The most typical structures present in this bed and related to subaerial exposure include rolled-up chips (Figure 4j: 'RC'), in-chip cracks (Figure 4j: 'ICC'), pyramid cracks (Figure 4j: 'PYC') and sheet crack (Figure 4j: 'SC'). The rolled-up chips, generally several mm thick and with rolled-up free edges originated from differential shrinkage accounted for by the humidity and contractibility gradient downward from the surface of the fine-grained sediments under subaerial condition, resembles what we commonly see in modern dried-up roadside puddles or ponds (Figure 5b).

Two kinds of cracks that are nearly always associated with rolled-up chips are pyramid cracks and in-chip cracks. The pyramid crack (Figure 4j: 'PYC') is the space between the free edges of laterally adjacent rolled-up chips and that under the rolled-up chips. They generally have a pyramidal top and a flat bottom. In the case that a series of pyramid cracks stacked, however, only the lowest one has a flat bottom, while others have pyramid bottoms (Figure 5b). In Bed 3, pyramid cracks and in-chip cracks are currently filled



DOI: 10.1002/gj

by blocky calcites. These kinds of cracks are distinguished from tectonic fissures by their unique shape, especially the nearly conical shape of the former.

The in-chip cracks (Figure 4j: 'ICC') occur in the lower part of the rolled-up chips. In vertical section, they have a wider lower end but a narrowing-up upper end, and are perpendicular to the lower side of the rolled-up chips. Their formation is related to the greater shrinkage in the upper part of the rolling-up chips. The formation of rolled-up chips, in-chip cracks and pyramid racks are all related to drying-up of fine-grained sediments under subaerial condition.

The other two types of cracks in Bed 3 are lateral cracks and vertical cracks. The former are parallel to bedding, and originated from previous bedding surfaces. This kind of crack is called 'sheet cracks' by Fischer (1964). Vertical cracks are those vertical to bedding, and are called 'prism cracks' by Fischer (1964) for the reason that they are generally polygonal in horizontal section, as shown in Figure 5d. Both of these kinds of cracks have an origination related to the dewatering shrinkage of fine-grained sediments in tidal-flat environments (Fischer 1964). The typical polygonal cross-section shape of prism cracks makes it easy for them to be distinguished from tectonic fissures.

The occurrence of rolled-up chips and various cracks in Bed 3 indicates that the fine-grained deposits of Bed 3 were exposed to subaerial conditions for a long time.

Examination of the thin sections from the top of Bed 3 reveals that the top surface of Bed 3 is an exposure surface (Figures 4h and i: 'SS'), which is characterized by the apatite debris (Figure 4i: 'AP') on the surface, which is assumed to be deposited under water, but to become debris under subaerial weathering conditions, and the vertical cracks cutting into the surface (Figure 4i: 'PC'), in which apatite debris and the same sediments as the overlying are present (Figure 4h: 'AP2'). The exposure surface indicates the occurrence of a sea-level fall event.

Bed 2 is platform facies, representing subtidal environments. The top exposure surface of Bed 3 represents a relative sea-level drop. Since Bed 3 is only 0.1 m thick, the change from the sedimentary environments of Bed 2 to that of Bed 3 is interpreted to be caused by a relative sea-level fall, instead of by sediment accumulation. The deposition of Bed 4 needs a small relative sea-level rise. Thus, there was a small relative-sea-level rise before the deposition of Bed 4.

Examinations of outcrops and thin sections reveal sheet cracks (Figure 5c: SC), prism cracks (Figure 5c: 'PC'), rolled-up chips (Figure 5c: 'RC') and pyramid cracks (Figure 5c: 'PYC') in Bed 4. All these cracks are filled by grey micritic deposits. The straight edges of the rolled-up chips, the nearly conical unique shape of the pyramid cracks in vertical section and the polygonal shape of the prism cracks in horizontal section (Figure 5d), as well as the micritic filling deposits in these cracks are the features to distinguish them from tectonic fissures or dissolution structures. The formation of all these cracks in Bed 4 may need another period of subaerial exposure, which may indicate another sea-level drop event.

Bed 7 contains abundant ammonoid and bivalves, representing a deeper normal marine environment. Bed 6 is a transition between Bed 5 and Bed 7, probably representing a shallow sublittoral environment. Bed 8 is characterized by thin flat beddings, representing a deeper and quiet marine environment.

## 4. DOLOSTONE-GYPSUM ASSEMBLAGE IN THE PTB SECTION AT SHITOUZHAI,ON A REEF-CORE SEQUENCE

### *4.1. Lithology*

The PTB section at Shitouzhai is divided into 4 beds (Figure 6a: '1'–'4'; Figure 3c). The basal Bed 1 is the top of the reef core sequence, composed of reef rock with reef-building calcisponges (Figures 7b and c: lower). Bed 2 is a dolostone composed of fine-crystalline, subhedral to euhedral dolomite crystals (Figures 7a and b: upper, 'Do'). No evidence is preserved about the precursor lithology of the dolostone. The contact between these two rocks is sharp, irregular and erosional. Our analyses show that the oxygen isotopic composition of the dolostone is much heavier than that of the underlying reef rocks.

The lithology of the lower part of Bed 3 (Figure 7f: '3-1'; Figure 6a: 'S3') has been divided into 4 layers: A, B, C and D (Figure 7d), each of which is several mm thick. The basal layers D and C are nonfossiliferous ML. Layer B is a dark grey, nonfossiliferous micritic limestone (ML) with abundant pseudomorphs of tabular gypsum crystals replaced by diagenetic calcite (Figure 7e). Even though the gypsum crystals have been generally replaced by calcite, their original tabular shape has been preserved. Layer A is a grey, nonfossiliferous ML.

The lithology of the upper part of Bed 3 (Figure 7f: '3-2', Figure 7f: 'S3U') has been divided into 4 layers: a, b, c and d (Figure 7g). The basal layer 'd' is a grey ML containing abundant pseudomorphs of gypsum crystals, each of which has been replaced by calcite crystals. Similar gypsum pseudomorphs have been observed in Ordovician rock in the Ordos Basin (Wu *et al*. 2006c). Layers 'c' and 'b' are grey ML, separated by a surface (Figure 7g: 'X'). There are many cracks in layers 'c' and 'b', which are all perpendicular to the surface 'X'.

Layer 'a' is a ML, containing more argillaceous mud and being brownish in colour. The lower part of layer 'a' contains many pseudomorphs of gypsum crystals replaced by calcite. Its middle part contains many bioclasts (Figure 7g: 'Bi'), all



DOI: 10.1002/gj


Figure 6. Outcrops of the Shitouzhai section. (a) Showing four beds of the section ('1'–'4') and locations of the samples ('S2' from both beds 1 and 2 and 'S3' from lower Bed 3, i.e. Sub-bed 3-1). Location of sample 'S3U' of upper Bed 3 (i.e. Sub-bed 3-2) is 1 m north to that of 'S3'. Bed 4 is covered by soils. (b) Another P–T boundary section 1 m from the Shitouzhai section, where Bed 2 is absent, showing the sharp contact between the reef rock of Bed 1 and the micritic limestone of Bed 3. (c) An outcrop of Bed 4 in a P–T boundary section 10 m north of the Shitouzhai section. This figure is available in colour online at www.interscience.wiley.com/journal/gj

severely recrystallized. The shapes of the bioclasts indicate that they seem to be fragments of gastropods and bivalves. The upper part of Layer 'a' is a yellowish lime mudstone containing argillaceous mud, which is overlain by the thin-bedded marls and shales (Figure 6c: '4') of the Lower Triassic Feixianguan Formation.

### 4.2. *Stratigraphy*

Bed 1 of this section contains a typical latest Permian reef fauna. The precursor rock of Bed 2 is unknown. Bed 3 is totally unfossiliferous except for possibly gastropod and bivalves bioclasts in its top part (Figure 7g: 'a'). Bed 4, the thin-bedded marls and shales of the Feixianguan Formation, has a wide distribution in this area and is generally assigned to the Early Triassic.

In the absence of conodonts, could the $\delta^{13}C$ curve be used to determine the P–T boundary? According to Jin *et al.* (2000), the $\delta^{13}C$ in the Meishan section has its lowest value in Beds 25 and 26. However, Bed 25 is claystone and 26 is marl, and their $\delta^{13}C$ values mainly reflect diagenetic calcites, rather than original sedimentary carbonates. Thus, they are better excluded in the chemostratigraphic analysis. If the $\delta^{13}C$ data of these two beds are excluded, the $\delta^{13}C$ value reaches its lowest point in the middle of Bed 27, that is, the beginning of the *Hindeodus parvus* Zone. Many other P–T boundary sections show the same trend: the $\delta^{13}C$ value dropped to its minimum at the base of the lowest Triassic conodont *Hindeodus parvus* Zone (Korte *et al.* 2004; Krull *et al.* 2004; Newton *et al.* 2004; Wang *et al.* 2007). Thus, in this paper the first lowest point of $\delta^{13}C$ value is tentatively used as an indication of the beginning of *H. parvus* Zone.

The present authors have tested the carbon isotopic composition of each sub-bed of Bed 3 (S3 and S3U) in the Laboratory of Ethan Grossman, Texas A & M University (Table 1; Figure 3C). The $\delta^{13}C$ values in Bed 3-1 (S3) range from 1.52 to 2.21 (‰, PDB), while those within Bed 3-2 (S3U) are 0.42∼−0.25. Thus, the P–T boundary in the Shitouzhai section is tentatively placed at between Bed 3-1 and Bed 3-2 (Figure 3C).



DOI: 10.1002/gj

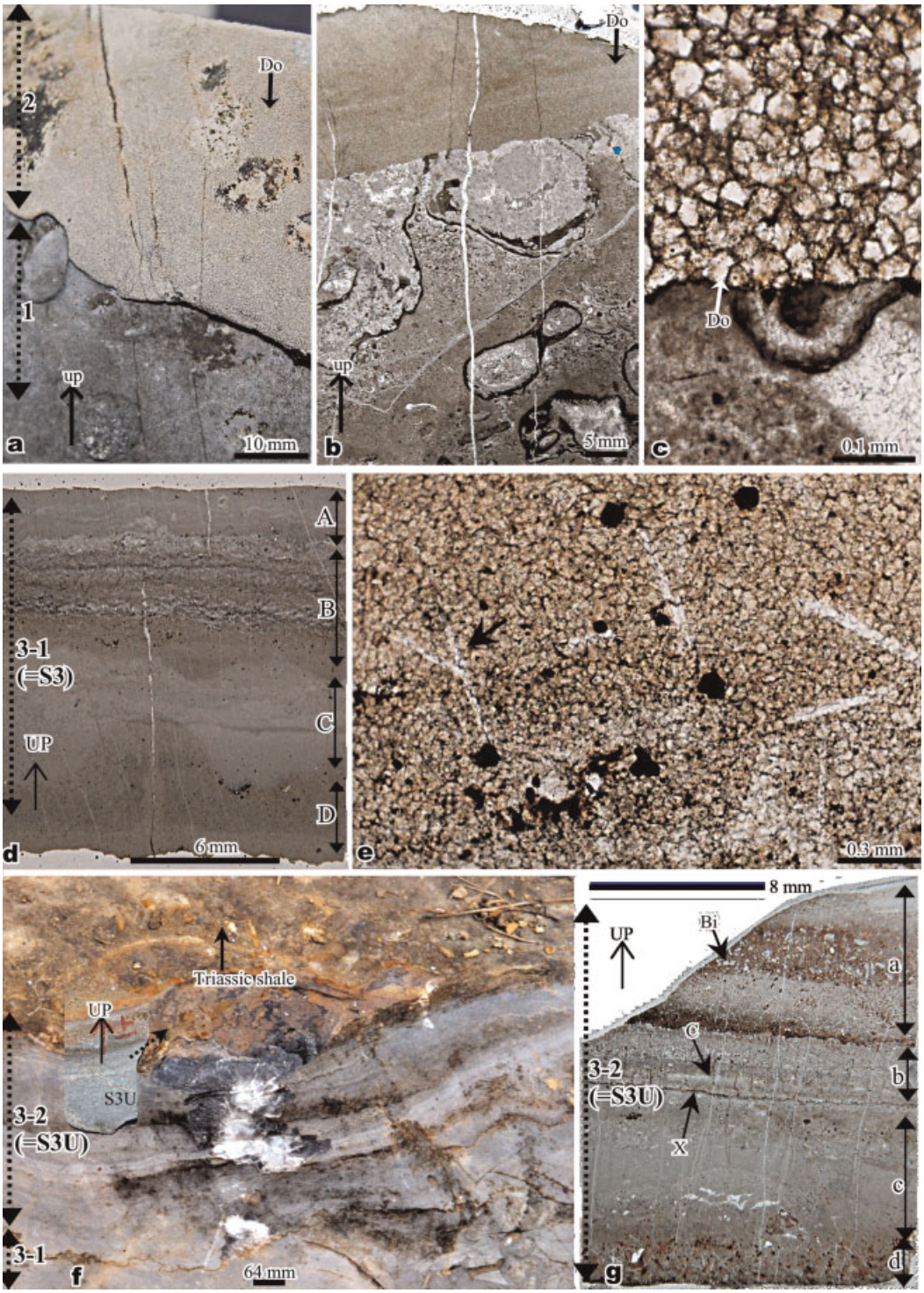


Figure 7. Lithology of the Shitouzhai section. (a) An outcrop of Beds 1 (lower) and 2 (upper) as sample S2. (b) Thin section showing reef rock of Bed 1 (lower) and dolostone of Bed 2 (upper: 'Do'). (c) Local enlargement of Figure 7b showing euhedral to subhedral dolomites of the dolostone ('Do') of Bed 2 and the reef rock of Bed 1 (lower). (d) Thin section of the Sub-bed 3-1 (sample S3), which has been divided into 4 layers (A, B, C and D), all nonfossiliferous micritic limestone, with abundant pseudomorphs of gypsum in Layer B. (e) Local enlargement of Layer B, showing tabular pseudomorphs of gypsum crystals replaced by calcite. (f) An outcrop of the Sub-bed 3-2 (Sample S3U). (g) Thin section of the Sub-bed 3-2, which has been divided into 4 layers (a, b, c and d), showing rich pseudomorphs of gypsum crystals replaced by calcite in the micritic limestone of layer 'd'. Layers 'b' and 'c' are micritic limestone. Layer 'a' consists of a lower micritic limestone with rich pseudomorphs of gypsum crystals replaced by calcite, a middle packstone/wackestone with recrystallized bioclasts probably of gastropods and bivalves and upper micritic limestone. This figure is available in colour online at www.interscience.wiley.com/journal/gj



DOI: 10.1002/gj

Table 1. Carbon and oxygen isotopic composition of samples from sub-beds of Beds 1 through 3 of the Shitouzhai section

| Sub-beds | Sample lithology | $\delta^{13}C$ (‰,PDB) | $\delta^{18}O$ (‰,PDB) |
|---|---|---|---|
| 3-2-a | Whole wackestone | −0.20 | −6.50 |
| 3-2-b | Black laminated micrites | −0.03 | −6.46 |
| 3-2-c | Grey micrites | 0.42 | −5.65 |
| 3-2-d | Grey micrites | −0.25 | −6.28 |
| 3-1-A | Grey micrites | 1.53 | −5.58 |
| 3-1-B | Laminated micrites | 1.52 | −5.77 |
| 3-1-C | Grey micrites | 2.21 | −5.38 |
| 3-1-D | Yellow micrites | 2.15 | −6.01 |
| 2-1 | Yellow fine dolostone | 3.03 | −3.54 |
| 2-2 | Micritic limestone | 2.72 | −7.1 |
| 1 | Micritic limestone | 2.43 | −7.19 |

### *4.3. Sedimentary environments and evidence for sea-level falls*

An irregular erosional surface is present on the top of Bed 1 (Figure 6b). The deposits on the erosional surface are micritic, differing from the underlying reef rock. The dolostone of Bed 2 overlying the reef rock of Bed 1 presents no reliable evidence for its precursor rock. It shows traces of a laminated structure. Its fine-crystalline fabric, composed of subhedral to euhedral dolomites generally with a dark centre and lighter edge, and its occurrence on top of a reef core, suggest that its formation may be related to evaporative supratidal environment. The heavier oxygen isotopic composition of the dolostone (Table 1: −3.54‰, PDB) than that of the underlying reef rock (−7.1‰, PDB) supports this interpretation. The irregular but sharp contact between the dolostone and reef rock, and the truncation of the sedimentary components and cements of the reef rock by the dolostone, suggest that the formation of the dolostone is later than the cementation of the reef. A reasonable interpretation is that the higher reef crest (Bed 1) once emerged out of sea water, after it is cemented by early aragonite, and suffered weathering, and then submerged into sea water and was covered by micritic deposits of Bed 3. The absence of Bed 2 in some places may represent subaerial erosion. The presence of gypsum crystals (pseudomorphs) in Bed 3, the dolomitization of the underlying Bed 2 and the monotonous micritic composition of Bed 3 suggest that Bed 3 may be formed in a supratidal haline environment. Regardless, the formation of the erosional surface on the top of the reef core facies needs a sea-level fall, and the formation of the gypsum in the micritic deposits of Bed 3 is attributed to the supratidal environments after the sea-level fall.

The PTB deposits at Shitouzhai are much thinner than those at Gendan, and are nonfossiliferous, which may be accounted for by the higher elevation of the reef crest during the deposition of Bed 3. The highest part of a reef will emerge out of sea water the earliest during a sea-level fall and submerge in sea water the latest during the following sea-level rise, which means the shortest time for deposition and smallest thickness of deposits in this area.

The association of the gypsum–bearing Bed 3 with the underlying dolostone of Bed 2 suggests some causal relationship between them: the precipitation of the gypsum crystals in the overlying micritic deposits because of evaporation under supratidal condition produced $Mg^{2+}$-rich brine, and the brine seeping into the underlying deposit caused the latter to be dolomitized (Adams and Rhodes 1960; Mckenzie 1981; Moore 1989). The total absence of any fossils from Bed 3 supports the interpretation that the sedimentary environment of Bed 3 may be supratidal.

## 5. DISSOLUTION BRECCIA IN PTB SECTION AT TANLUZHAI, BACK-REEF SEQUENCE

### *5.1. Lithology*

The PTB section at Tanluzhai has been divided into 6 beds (Figure 3D). The Bed T11 underlying Bed 0 are reef rocks containing *Palaeofusulina sinensis*. Beds 0–3 are non-reef deposits and contain no fusulinid fossils. Bed 4 contains the Early Triassic ammonoid *Ophiceras*.

Bed 0 is a limestone with laminated structure and small molluscs. Bed 1 is a fine-crystalline dolostone with laminated structure and small molluscs. Its precursor rock may be the same as Bed 0. Bed 2 is a breccia consisting of fragments of a dolostone similar to Bed 1 (Figure 8b: 'DF') and grey ML matrix (Figure 8b: 'ML'). As observed at the outcrops (Figure 8b), many of the dolostone fragments (DF) are preserved aligned in the same direction. In some places, the dolostone beds are elongate and stretch horizontally (Figure 8a), with the space between them filled by grey micrites. The dolostone consists of subhedral to euhedral, fine-crystalline dolomites. Our analyses show that the dolostone has an oxygen isotopic composition (−3.64‰, PDB) heavier than that of the limestone of Bed 0 (−4.47‰, PDB). Locally, CCC occur between DF (Figure 8c).

Bed 3 is a fine-crystalline dolostone (Figure 8d) composed of euhedral to subhedral dolomites (Figure 8e), with wavy laminated structure (Figure 8d) probably related to an algal mat origin. Bed 4 is a limestone containing clays and is yellowish in colour. X-ray diffraction analysis shows that the clays are mainly illite. It may be the illite that causes the limestone to appear yellowish. The yellowish limestone contains some Early Triassic ammonoids. Bed 5 contains abundant Early Triassic ammonoids (Figure 8f).



DOI: 10.1002/gj

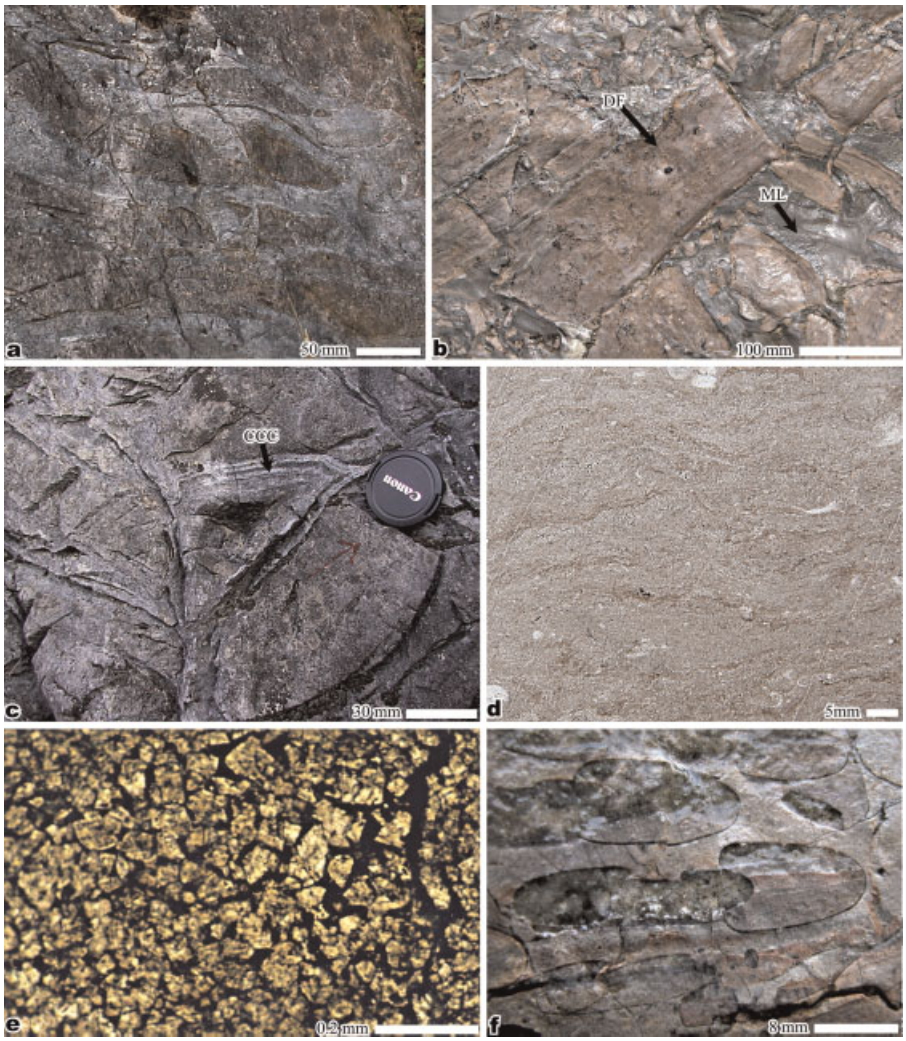


Figure 8. Lithology of the Tanluzhai section. (a) An outcrop of Bed 2, showing grey micritic fillings in space assumed formed from dissolution of previous evaporate interbeds between brownish laminated dolostone beds. (b) An outcrop of lower and middle Bed 2, showing dolostone fragments (DF) mostly *in situ* and the nonfossilferous micritic limestone (ML) matrix between the DF. (c) An outcrop of upper Bed 2, showing crustose multi-generational calcite cements (CCC) between the DF. (d) Thin sections of Bed 3, fine-crystalline dolostone with laminated structure. (e) Enlargement of Figure 8d, showing subhedral to euhedral dolomite crystals. (f) An outcrop of Bed 5, showing ammonoids. This figure is available in colour online at www.interscience.wiley.com/journal/gj

### *5.2. Stratigraphy*

Bed T11 is a reef facies containing Upper Permian Changhsingian fusulinid fossils, and is correlative to Bed 2 of the Gendan sections, as well as Bed 1 of the Shitouzhai section, both of which also contain Upper Permian Changhsingian fusulinid fossils. Beds 0 and 1 contain a biota composed of small molluscs. A change in biota from reefal type to non-reef type occurred in all three sections, and may represent a roughly coeval event boundary. Thus, the boundary between Bed T11 and Bed 0 of the Tanluzhai section is correlated to that between Beds 1 and 2 of the Shitouzhai section, and to that between Beds 2 and 3 of the Gendan section. The biota of Bed 4 of the Tanluzhai section is characterized by normal-sized ammonoids, representing normal marine environments. The same or similar biota occurs in Bed 7 of the Gendan section. Thus, the boundary between Beds 3 and 4 of the Tanluzhai section is correlated to that between Beds 6 and 7 of the Gendan section. Bed 4 of the Shitouzhai section is nonfossiliferous, and is correlated to Bed 8 of the Gendan section, which is also nonfossiliferous. Beds 0 through 3 of the Tanluzhai section are correlated to Beds 2 and 3 of the Shitouzhai section. In the absence of conodont fossils, it is difficult to accurately determine the P–T boundary in the Tanluzhai section.



DOI: 10.1002/gj

### 5.3. Sedimentary environments

The top of the back-reef sequence (Figure 8: 'T11') underlying Bed 0 is a framestone, which represent normal marine environment less than 20 m deep (Wu and Fan 2000). Beds 0 and 2 contain only small molluscs and algal laminated structures, without any components of reefal biota of Bed T11. The composition of this biota is most probably related to a tidal environment, which generally excludes all stenotropic organisms but eurytropic molluscs (commonly small-sized) and algal mats. The fine-crystalline, euhedral to subhedral fabric of Bed 1, as well as its occurrence on a back-reef sequence suggest an origin possibly related to supratidal evaporative environment (Moore 1989). The nearly *in situ* arrangement of the DF in Bed 2 indicates that they may form from the collapse of thin-bedded dolostone, on the condition that some evaporite interbeds, such as gypsum layers, previously intercalating with the thin-bedded dolostone, were removed out by dissolution. This interpretation needs a supratidal evaporative environment for the formation of the once present evaporite interbeds. The dolostone lithology of the underlying Bed 1 and the overlying Bed 3, as well as the laminated fine-crystalline dolomite composition of the DF is in agreement with the interpretation. Supposing that Bed 2 represents a supratidal evaporative environment, the change from the sedimentary environment of Bed T11 to that of Bed 2 requires a relative sea-level fall.

If the assumption of evaporite interbeds is untrue, the DF could have formed in a weathering event such as a calichification. The matrix between the DF in the lower and middle parts of Bed 2 is ML. In the upper part of Bed 2, however, it is crustose calcite cement (Figure 8c: 'CCC'). Our tests reveal that the CCC has an oxygen isotopic composition of −5.06‰ (PDB) at the base and −2.9‰ at the distal end. Such an oxygen isotopic composition pattern indicates an origin in an open evaporative environment. Thus, it is probable that a calichification event related to subaerial exposure has caused the dissolution of the evaporative interbeds, the collapse of the dolostone beds, as well as the formation of the crustose cement. The presence of algal laminated structures and absence of fossils in Bed 3 suggests that Bed 3 may be a tidal-flat deposit. The fine-crystalline, euhedral to subhedral fabric in Bed 3 (Figures 8d and e) suggests dolomitization in an evaporative supratidal environment (Moore 1989). The ammonoids in Bed 4 (Figure 8f) and Bed 5 indicate relatively deeper-water, normal marine conditions.

## 6. DISCUSSION

Wu *et al.* (2003) reported a sea-level fall in the latest Permian in Ziyun, Guizhou Province, South China. However, Fang (2004) denied any sea-level falls in the latest Permian, and suspected the latest Permian timing of the sea-level fall in Ziyun because of the absence of conodonts in timing the sea-level fall in Wu and Fan's (2000) paper. In the current paper, critical conodonts for a biostratigraphic framework have been found in the Gendan section, and carbon isotopic stratigraphy has been used in determining the P–T boundary in the Shitouzhai section. A sequence stratigraphic correlation has been achieved among the three sections. All these works have established a basic stratigraphic framework for the three sections. Thus, at this moment, we can make such an inference that in the Ziyun area, a sea-level fall really occurred during the latest Permian, between the *Clarkina yini* and *Hindeodus parvus* zones. The researchers who suspect the occurrence of sea-level falls in the latest Permian are expected to explain the case in Ziyun.

Interestingly, we are not the only workers who have found evidence for sea-level falls in Ziyun. For example, Lu *et al*. (1999) reported deep erosional cuttings in the top of the Upper Permian Changhsingian reef in Ziyun. Wei and Enos (1991) and Enos *et al*. (2007) noticed a probable palaeokarst surface of about 10 m relief on the top of the Ziyun reef. Our research results are in accordance with their results, but show more details.

A large sea-level fall causes down-shift of onlap. Jin *et al*. (1994, 1995) reported up-shift of onlap in the Sichuan-Hubei area during the Changhsingian Stage. Their result was used as evidence for a continuous sea-level rise from the latest Permian to the earliest Triassic by some researchers (Hallam and Wignall 1997). However, according to Zhang *et al*. (2002), the onlap in the Meishan area of Zhejiang Province in the Changhsingian Stage and Griesbachian Substage includes two down-shifts at the middle and the end of the Changhsingian Stage, respectively. The work of Jin *et al*. (1994, 1995) was completed before a high-resolution biostratigraphic framework for the P–T boundary strata had been established. Zhang *et al*.'s (2002) work has a high-resolution conodont biostratigraphic basis, and appears to be more robust.

In recent years, more and more P–T boundary sections have been found to contain geological records of a sea-level fall in the latest Permian. For example, Wu *et al*. (2006a) reported evidence for a sea-level fall in the latest Permian in a P–T boundary section in Xiushui, Jiangxi Province, South China. Wu *et al*. (2006b) also reported evidence for sea-level falls in the latest Permian in the P–T boundary section at Laolongdong, Chongqing (previously belonging to the Sichuan Province). It is based on their study on the P–T boundary section at Laolongdong that Wignall and Hallam (1996) proposed that there was no sea-level fall in the latest Permian, but a sea-level rise beginning in the latest Permian and lasting into the early Triassic. The critical evidence in



DOI: 10.1002/gj

the Laolongdong section found by Wu *et al*. (2006b) is undulate erosional surfaces. Similar evidence is present in the P–T boundary section in Huaying area, Sichuan Province (Ezaki *et al*. 2003) and in the P–T boundary section in Langpai area, Luodian, Guizhou Province, South China (Ezaki *et al*. 2008).

Zhang *et al*. (2006) studied the P–T boundary section at Dongpan, Guangxi Province, South China, and found that a large sea-level fall had occurred at the horizon roughly correlated to the middle of Bed 24e of the Meishan section, the GSSP of the P–T boundary. According to the palaeoecology of the radiolarian faunas, they determined the sea-level fall has a magnitude of more than 150 m, which is much greater than that in the Ziyun area, as determined by Wu *et al.* (2003) using the diagenetic structures in the Changhsingian reefs in Ziyun.

Not only in China has evidence for a sea-level fall been found in the latest Permian, but also in the P–T boundary sections in other places of the world. For example, Farabegoli *et al*. (2007) found two unconformity surfaces in the latest Permian of the Bulla and Tesero sections in the Southern Alps (Italy). In the Tesero section, the first (lower) unconformity surface is about 2 m below the P–T boundary, as determined by the base of the *Hindeodus parvus* Zone, and the second (upper) one is about 1.5 m below the P–T boundary. The uppermost 2.6 m of rock beneath the lower unconformity surface contains root traces, indicating exposure to subaerial conditions. The interval between the upper unconformity and the P–T boundary contains conodonts and abundant ooids, indicating shallow subtidal environments. The shallow water conditions continued a little up into the basal part of the *Hindeodus parvus* Zone.

Heydari *et al*. (2003) presented geochemical and mineralogical evidence for 'a rapid and major drop in relative sea-level at or just before the P–T boundary' in the PTB section in Abadeh, Iran. However, Fang (2005) and Wignall *et al*. (2005) disagreed with them. The present authors agree with Heydari *et al*. (2003; Heydari 2005) that Unit 7 represents a deep water environment, and believe that the sedimentary environment of the crystal fan layer is unclear, and we do not agree with Fang's (2005) microbialite interpretation for it. The lithology of the 'peloid layer' is difficult to determine before more work is done. We agree that the lime mudstone overlying the 'peloid layer' represents a deep water environment, and believe that the evidence for a sea-level fall, if it really exists, should be present in the 0.5 m wackestone underlying the 'peloid layer' and/or in the crystal fan layer.

Sea-level changes can be relative or eustatic. Before it is confirmed to be the latter, it is assumed to be the former. A relative sea-level rise can be the effect of a substantial basinal subsidence or a eustatic sea-level rise, while a relative sea-level fall can be the result of a tectonic uplift of the basin bottom, or a eustatic sea-level fall. It is difficult to distinguish a relative sea-level change from a eustatic one. However, there is a basic rule, that is, if a sea-level change is relative, it has impact only in a local area, while a eustatic sea-level change has worldwide impact: it will leave a similar geological record in many sites (sections) throughout the world. Are the sea-level changes found in the latest Permian of the P–T boundary section in Ziyun relative or eustatic? Since more and more P–T boundary sections over the world have been found to contain geological records of sea-level falls in the latest Permian, they can be eustatic. Of course, this need to be confirmed by more studies on P–T boundary sections in other places.

To determine the sea-level changes during the P–T transition is important, because they may be the cause of the end-Permian mass extinctions. Wignall and Hallam (1992) proposed that it is the oceanic anoxia caused by the sea-level rise continuing from the latest Permian to the early Triassic that caused the mass extinction in the P–T transition. However, this study and many other studies are challenging Wignall and Hallam's (1992) belief that there was no sea-level fall during the latest Permian. The reality is that there may well be eustatic sea-level falls during the latest Permian.

Eustatic sea-level changes can be the results of (1) changes in the total volume of oceanic water on the earth because of drastic global climatic changes, and (2) changes in the total volume of the oceanic crust because of changes in the expanding speed of oceanic ridges. A drastic global climatic cooling can cause increase in the total volume of glaciers on the earth, and the resultant decrease in the total volume of oceanic water on the earth, which appear as a eustatic sea-level fall and can be recorded in deposits in geological time. If a eustatic sea-level fall occurred during the latest Permian, they could be caused by some drastic climatic cooling events. Any drastic climatic cooling events can cause mass extinction of stenotropic organisms. Wu (2005) and Wu *et al*. (2007b) have found that the mass extinction of reef ecosystems in the P–T transition happened in two steps. The first is the sudden disappearance of all stenotropic organisms including calcisponges and fusulinids in the *Clarkina yini* Zone, and second is the disappearance of most eurytropic organisms including microgastropods and algal mats at the beginning of the *Hindeodus parvus* Zone. Wu *et al*. (2007b) also found that the occurrence of the first step of the mass extinction is coeval with the first sea-level fall event, which is in agreement with the findings by Yin *et al*. (2007) that the prelude of the end-Permian mass extinction commenced during the time between Beds 24e and 25 at Meishan and coincided with the end-Permian regression. Non-reef ecosystems have an extinction pattern similar to that of reef ecosystems (Wu *et al*. 2007b). Wu (2005) has studied the ecological selection in the end-Permian mass extinction, and found that the extinct taxa are



DOI: 10.1002/gj

almost all warm-water types, while those surviving the end-Permian crisis are all eurytropic types. This fact supports the hypothesis that the mass extinction which happened during the P–T transition may have been caused by some drastic climatic cooling events, which have caused substantial eustatic sea-level falls.

## 7. CONCLUSIONS

(1) Study of three Permian-Triassic boundary sections on the Upper Permian Changhsingian reef in Ziyun, Guizhou Province, South China reveals evidence for sea-level falls. It includes:
   (a) Tabular gypsum pseudomorphs in one bed in the P–T transition on the reef-core sequence and the dolostone of the underlying bed, a combination of both indicating that once there was a supratidal sedimentary-diagenetic environment;
   (b) Various desiccation cracks and an exposure surface in the P–T transition on the reef-front sequence, whose formation is attributed to a sea-level fall;
   (c) Breccia in the P–T transition on the back-reef sequence, whose origin may be related to the collapse of the thin dolostone beds, on the condition that the former evaporite interbeds such as gypsum layers were removed by dissolution.

(2) Evidence for sea-level falls in the latest Permian has also been found in Chongqing, Jiangxi and many other places. Thus, the sea-level falls in the latest Permian may be eustatic, even though this conclusion is not the final statement.

## ACKNOWLEDGEMENTS

This study was funded by the National Natural Science Foundation of China (Project Nos. 40802001 and 40472015), the Science Foundation of China Postdoctors (Grant No. 20070420523) and the State Key Laboratory of Modern Paleontology and stratigraphy (Grant No. 083113). Steve Kershaw, Ethan Grossman, Thomas Yancey and BO Slone have revised the earlier versions of this paper, and two reviewers have provided us with very constructive comments. Ian Somerville, Charles Henderson and Shuzhong Shen have corrected the recent version of this paper and greatly improved its English. Sincere thanks go to all of them.

## REFERENCES

**Adams JE, Rhodes ML. 1960**. Dolomitization by seepage refluxion. *AAPG Bulletin* **44**: 1912–1920.

**Benton MJ, Tverdokhlebov VP, Surkov MV. 2004**. Ecosystem remodeling among vertebrates at the Permian-Triassic boundary in Russia. *Nature* **432**: 97–100.

**Brookfield ME, Twitchett RJ, Gooding C. 2003**. Palaeoenvironments of the Permian-Triassic transition sections in Kashmir, India. *Palaeogeography, Palaeoclimatology, Palaeoecology* **198**: 353–371.

**Enos P, Lehrmann DJ, Wei JY, Yu YY, Xiao JF, Chaikin DH, Minzoni M, Berry AK, Montgomery P. 2007**. Triassic evolution of the Yangtze Platform in Guizhou Province, P.R.C. *Geological Society of America, Special Paper* **417**: 1–105.

**Erwin DH, Bowing SA, Jin YG. 2002**. End-Permian mass extinctions: a review. *GSA Special Paper* **356**: 363–383.

**Eshet Y, Rampino MR, Visscher H. 1995**. Fungal event and palynological record of ecological crisis and recovery across the Permian-Triassic boundary. *Geology* **23**: 967–970.

**Ezaki Y, Liu J, Adachi N. 2003**. Earliest Triassic microbialite micro to megastructures in the Huaying area of Sichuan Province, south China: implications for the nature of oceanic conditions after the end-Permian extinction. *Palaios* **18**: 388–402.

**Ezaki Y, Liu JB, Nagano T, Adachi N. 2008**. Geobiological aspects of the earliest Triassic microbialites along the southern periphery of the tropical Yangtze platform: initiation and cessation of a microbial regime. *Palaios* **23**: 356–369.

**Fang ZJ. 2004**. The Permian-Triassic boundary crisis: pattern of extinction, collapse of various ecosystems, and their causes. In *Mass Extinction and Recovery Evidences from the Palaeozoic and Triassic of South China*, Rong JY, Fang ZJ (eds). University of Science and technology of China Press: Hefei; 785–928.

**Fang ZJ. 2005**. Comment on Permian–Triassic boundary interval in the Abadeh section of Iran with implications for mass extinction: Part 1—: sedimentology by E. Heydari, J. Hassanzadeh, W.J. Wade and A.M. Ghazi, Palaeogeography, Palaeoclimatology, Palaeoecology, 193: 405-424 (2003): A. *Palaeogeography, Palaeoclimatology, Palaeoecology* **217**: 311–313.

**Farabegoli E, Perri MC, Posenato R. 2007**. Environmental and biotic changes across the Permian–Triassic boundary in western Tethys: the Bulla parastratotype, Italy. *Global and Planetary Change* **55**: 109–135.

**Fischer AG. 1964**. The lofer cyclothems of the Alpine Triassic. *Kansas Geological Survey Bulletin* **169**: 107–149.

**Garzanti E, Nicora A, Rettori R. 1998**. Permo-Triassic boundary and lower to middle Triassic in south Tibet. *Journal of Asian Earth Sciences* **16**: 143–157.

**Grice K, Cao CQ, Love GD, Bottcher ME, Twitchett RJ, Grosjean E, Summons RE, Turgeon SC, Dunning W, Jin YG. 2005**. Photic zone euxinia during the Permian-Triassic superanoxic event. *Science* **307**: 706–709.

**Hallam A, Wignall PB. 1997**. *Mass Extinction and Their Aftermath*. Oxford University Press: 125–126.

**Heydari E, Hassanzadeh J, Wade WJ, Ghazi AM. 2003**. Permian-Triassic boundary interval in the Abadeh section of Iran with implications for mass extinction: Part 1-Sedimentology. *Palaeogeography, Palaeoclimatology, Palaeoecology* **193**: 405–423.

**Heydari E. 2005**. Reply to the comments on Permian–Triassic boundary interval in the Abadeh section of Iran with implications for mass extinction: Part 1: sedimentology by E. Heydari, J. Hassanzadeh, W.J. Wade and A.M. Ghazi, Palaeogeography, Palaeoclimatology, Palaeoecology, 193:405-424 (2003): Reply. *Palaeogeography, Palaeoclimatology, Palaeoecology* **217**: 319–325.

**Isozaki Y. 1997**. Permo-Triassic boundary superanoxia and stratified superocean: records from lost deep sea. *Science* **276**: 235–238.

**Jin YG, Shen SZ, Zhu ZL, Mei SL, Wang W. 1996**. The Selong section, candidate of the Global Stratotype section and point of the Permian-Triassic boundary, In *The Palaeozoic-Mesozoic Boundary*. Yin HF (ed.). China University of Geosciences Press: Wuhan; 127–137.

**Jin Y.G., Wang Y, Shang QH, Cao CQ, Erwin DH. 2000**. Pattern of marine mass extinction near the Permian-Triassic boundary in south China. *Science* **289**: 432–436.

**Jin YG, Zhang J, Shang QH. 1994**. Two phases of the end-Permian mass extinction, In *Pangea: Global Environments and Resources*. Embry AE,

Beauchamp B, Glass DJ (eds). Canadian Society of Petroleum Geologists Calgary. Memoir; **17**: 813–822.

**Jin YG, Zhang J, Shang QH. 1995**. Pre-Lopingian catastrophic event of marine faunas. *Acta Palaeontologica Sinica* **34**(4): 410–427.

**Kajiwara Y, Yamakita S, Ishida K, Ishiga H, Imai A. 1994**. Development of a largely anoxic stratified ocean and its temporary massive mixing at the Permian/Triassic boundary supported by the sulfur isotopic record. *Palaeogeography, Palaeoclimatology, Palaeoecology* **111**: 367–379.

**Kershaw S, Guo L, Swift A, Fan JS. 2002**. Microbialites in the Permian-Triassic boundary interval in central China: structure, age and destruction. *Facies* **47**: 83–90.

**Kershaw S, Zhang TS, Lan GZ. 1999**. A microbialite carbonate crust at the Permian-Triassic boundary in South China, and its palaeoenvironmental significance. *Palaeogeography, Palaeoclimatology, Palaeoecology* **146**: 1–18.

**Korte C, Kozur HW, Partoazar H. 2004**. Negative carbon isotope excursion at the Permian-Triassic boundary section at Zal, NW-Iran. *Hallesches Jahrbüch Geowissenshaft, Reihe B* **18**: 69–71.

**Krull ES, Lehrmann DJ, Druke D, Kessel B, Yu YY, Li RX. 2004**. Stable carbon isotope stratigraphy across the Permian-Triassic boundary in shallow marine carbonate platforms, Nanpanjiang Basin, south China. *Palaeogeography, Palaeoclimatology, Palaeoecology* **204**: 297–315.

**Krystyn L, Richoz S, Baud A, Twitchett RJ. 2003**. A unique Permian-Triassic boundary section from the Neotethyan Hawasina Basin, central Oman Mountains. *Palaeogeography, Palaeoclimatology, Palaeoecology* **191**: 329–344.

**Lai XL, Yang FQ, Hallam A, Wignall PB. 1996**. The Shangsi section, candidate of the Global Stratotype section and point of the Permian-Triassic boundary, In *The Palaeozoic-Mesozoic Boundary.* Yin HF (ed.). China University of Geosciences Press: Wuhan; 113–126.

**Lehrmann DJ, Payne JL, Felix SV, Dillett PM, Wang HM, Yu Y, Wei J. 2003**. Permian-Triassic boundary sections from shallow-marine carbonate platforms of the Nanpanjiang Basin, south China: implications for oceanic conditions associated with the end-Permian extinction and its aftermath. *Palaios* **18**: 138–152.

**Lehrmann DJ, Yang W, Wei JY, Yu YY, Xiao JF. 2001**. Lower Triassic peritidal cyclic limestone; an example of anachronistic carbonate facies from the Great Bank of Guizhou, Nanpanjiang Basin, Guizhou Province, South China. *Palaeogeography, Palaeoclimatology, Palaeoecology* **173**(3–4): 103–123.

**Lehrmann DJ, Wei JR, Enos P. 1998**. Controls on facies architecture of a large Triassic carbonate platform: the Great Bank of Guizhou, Nanpanjiang Basin, South China. *Journal of Sedimentary Research* **68**(2): 311–326.

**Lu YC, Li ST, Ye HB, Zhou YQ. 1999**. Effect of sea level changes on Ziyun reef accretion in Guizhou Province, China. *Earth Science-Journal of China University of Geosciences* **24**(6): 585–589.

**Mckenzie JA. 1981**. Holocene dolomitization of calcium carbonate sediments from the coastal sabkhas of Abu Dhabi, U.A.E.: a stable isotope study. *Journal of Geology* **89**: 185–198.

**Mei SL, Zhang KX, Wardlaw BR. 1998**. A refined succession of Changhsingian and Griesbachian neogondolellid conodonts from the Meishan section, candidate of the global stratotype section and point of the Permian-Triassic boundary. *Palaeogeography, Palaeoclimatology, Palaeoecology* **143**: 213–226.

**Michaelsen P. 2002**. Mass extinction of peat-forming plants and the effect on fluvial styles across the Permian-Triassic boundary, northern Bowen Basin, Australia. *Palaeogeography, Palaeoclimatology, Palaeoecology* **179**: 173–188.

**Moore CH. 1989**. *Carbonate Diagenesis and Porosity.* Elsevier: Amsterdam -Oxford- New York-Tokyo.

**Newton RJ, Pevitt EL, Wignall PB, Bottrell SH. 2004**. Large shifts in the isotopic composition of seawater sulphate across the Permo–Triassic boundary in northern Italy. *Earth and Planetary Science Letters* **218**: 331–345.

**Noé SU. 1987**. Facies and paleogeography of the marine Upper Permian and of the Permian-Triassic boundary in the southern Alps (Bellerophon Formation, Tesero Horizon). *Facies* **16**: 89–142.

**Peng YQ, Zhang SX, Yu TX, Yang FQ, Gao YQ, Shi GR. 2005**. High-resolution terrestrial Permian-Triassic eventostratigraphic boundary in western Guizhou and eastern Yunnan, southwestern China. *Palaeogeography, Palaeoclimatology, Palaeoecology* **215**: 285–295.

**Retallack GJ. 1995**. Permian-Triassic life crisis on land. *Science* **267**: 77–80.

**Retallack GJ, Seyedolali A, Krull ES, Holser WT, Ambers CP, Kyte FT. 1998**. Search for evidence of impact at the Permian-Triassic boundary in Antarctica and Australia. *Geology* **26**: 979–982.

**Schubert JK, Bottjer DJ. 1995**. Aftermath of the Permian–Triassic mass extinction event: paleoecology of Lower Triassic carbonates in the western USA. *Palaeogeography, Palaeoclimatology, Palaeoecology* **116**: 1–39.

**Shen SZ, Jin YG. 1999**. Brachiopods from the Permian-Triassic boundary beds at the Selong Xizang section, Xizang (Tibet), China. *Journal of Asian Earth Sciences* **17**: 547–559.

**Shen JW, Xu HL. 2005**. Microbial carbonates as contributors to Upper Permian (Guadalupian–Lopingian) biostromes and reefs in carbonate platform margin setting, Ziyun County, South China. *Palaeogeography, Palaeoclimatology, Palaeoecology* **218**: 217–238.

**Steiner MB, Eshet Y, Rampino MR, Schwindt DM. 2003**. Fungal abundance spike and the Permian-Triassic boundary in the Karoo Supergroup (South Africa). *Palaeogeography, Palaeoclimatology, Palaeoecology* **194**: 405–414.

**Tong JN, Yin HF, Zhang KX. 1999**. Permian and Triassic sequence stratigraphy and sea-level changes of eastern Yangtze platform. *Journal of China University of Geosciences* **10**: 161–169.

**Twitchett RJ, Krystyn L, Baud A, Wheeley JR, Richoz S. 2004**. Rapid marine recovery after the end-Permian mass extinction event in the absence of marine anoxia. *Geology* **32**: 805–808.

**Twitchett RJ, Looy CV, Visscher H, Wignall PB. 2001**. Rapid and synchronous collapse of marine and terrestrial ecosystems during the end-Permian biotic crisis. *Geology* **29**: 351–354.

**Wang SH, Fan JS, Rigby JK. 1996**. The characteristics and development of the Permian reefs in Ziyun County, South Guizhou, China. *Acta Sedimentologica Sinica* **14**: 66–74.

**Wang W, Hano A, Okumura T, Ma YS, Matsumoto R, Matsuda N, Ueno K, Chen XZ, Kakuwa Y, Gharaie MHM, Ilkhchi MR. 2007**. Isotopic chemostratigrahpy of the microbialite-bearing Permian-Triassic boundary section in the Zagros Mountains, Iran. *Chemical Geology* **244**: 708–714.

**Ward PD, Botha J, Buick R, De Kock MO, Erwin DH, Garrison GH, Kirschvink JL, Smith R. 2005**. Abrupt and gradual extinction among late Permian land vertebrates in the Karoo Basin, South Africa. *Science* **307**: 709–714.

**Wignall PB, Hallam A. 1992**. Anoxia as a cause of the Permian/Triassic mass extinction: facies evidence from northern Italy and the western United States. *Palaeogeography, Palaeoclimatology, Palaeoecology* **93**: 21–46.

**Wignall PB, Hallam A. 1996**. Facies change and the end-Permian mass extinction in S.E. Sichuan, China. *Palaios* **11**: 587–596.

**Wignall PB, Newton R. 2003**. Contrasting deep-water records from the Upper Permian and Lower Triassic of south Tibet and British Columbia: evidence for a diachronous mass extinction. *Palaios* **18**: 153–167.

**Wignall P, Woods A, Bottjer D. 2005**. Comment on Permian–Triassic boundary interval in the Abadeh section of Iran with implications for mass extinction: Part 1: sedimentology by E. Heydari, J. Hassanzadeh, W.J. Wade and A.M. Ghazi, Palaeogeography, Palaeoclimatology, Palaeoecology, 193:405-424(2003): B. *Palaeogeography, Palaeoclimatology, Palaeoecology* **217**: 315–317.

**Wu YS. 2005**. *Conodonts, Reef Evolution and Mass Extinction Across Permian-Triassic Boundary.* Geological Publishing House: Beijing; 1–90.

**Wu YS, Fan JS. 2000**. Paleoecology of calcisponges. *Acta Paleontologica Sinica* **39**(4): 544–547.

**Wu YS, Fan JS, Jin YG. 2003**. Emergence of the Late Permian changhsingian reefs at the end of the Permian. *Acta Geologica Sininca* **77**(3): 289–296.

**Wu YS, He SL, Lu T, Da SP, Li YG, Dai YD. 2006c**. Diagenetic patterns and pore systems of the Lower Ordovician Majiagou Formation reservoirs of the central Changqing gas fields. *Acta Petrologica Sinica* **22**(8): 2171–2181.

**Wu YS, Jiang HX, Yang W, Fan JS. 2007a**. Microbialite of anoxic condition from Permian-Triassic transition in Guizhou, China. *Science in China Series D* **50**(7): 1040–1051.

**Wu YS, Yang W, Jiang HX, Fan JS. 2006a**. Petrologic evidence for sea-level drop in the latest Permian in Jiangxi Province, China, and its meanings for mass extinction. *Acta Petrologica Sinica* **22**(12): 3039–3046.

**Wu YS, Jiang HX, Liao TP. 2006b**. Sea-level drops in the Permian-Triassic boundary section at Laolongdong, Chongqing, Sichuan Province. *Acta Petrologica Sinica* **22**(9): 2405–2412.

**Wu YS, Fan JS, Jiang HX, Yang W. 2007b**. Extinction pattern of reef ecosystems in latest Permian. *Chinese Science Bulletin* **52**(4): 512–520.

**Xie SC, Pancost RD, Yin HF, Wang HM, Evershed RP. 2005**. Two episodes of microbial change coupled with Permo/Triassic faunal mass extinction. *Nature* **434**: 494–497.

**Yang ZY, Wu SB, Yin HF, Xu GR, Zhang KX, Bi XM. 1991**. *Permo-Triassic Events of South China*. Geological Publishing House: Beijing; 1–153.

**Yin HF, Zhang KX, Tong JN, Yang ZY, Wu SB. 2001**. The Global Stratotype Section and Point (GSSP) of the Permian-Triassic Boundary. *Episodes* **24**(2): 102–114.

**Yin HF, Wu SB, Ding MH, Zhang KX, Tong JN, Yang FQ, Lai XL. 1996**. The Meishan section, candidate of the global stratotype section and point of Permian-Triassic boundary, In *The Palaeozoic-Mesozoic Boundary.* Yin HF (ed.). China University of Geosciences Press: Wuhan; 31–48.

**Yin HF Feng QL Lai XL Baud A Tong JN 2007** The protracted Permo-Triassic crisis and multi-episode extinction around the Permian–Triassic boundary *Global and Planetary Change* **55** 1–20

**Zhang F, Feng QL, Meng YY, He WH, Gu SZ. 2006**. Stratigraphy of organic carbon isotope and associated events across the Permian-Triassic boundary in the Dongpan deep-water section in Liuqiao area, Guangxi, South China. *Geoscience* **20**(1): 42–48.

**Zhang KX, Tong JN, Hou JG, Wu SB, Zhu YH, Lin QX, Gu YS, Yuan YB, Han ZJ, Peng YQ., 2002**. *Geological Map of Meishan Town, The People's Republic of China*. China University of Geosciences Press Wuhan.




DOI: 10.1002/gj